JOURNAL OF SPACECRAFT AND ROCKETS
Vol. 36, No. 6, November–December 1999

Modeling and Nonlinear Structural Analysis of a Large-Scale Launch Vehicle

Richard D. Young*
Lockheed Martin Engineering and Sciences Services, Hampton, Virginia 23681-2199
and
Charles C. Rankin†
Lockheed Martin Missiles and Space Company, Palo Alto, California 94304-1191

Advanced modeling and analysis capabilities of a state-of-the-art general purpose finite element code, developed for nonlinear structural analysis of launch vehicles, are described. In particular, the application of these capabilities to nonlinear analyses of the new Space Shuttle superlightweight external liquid-oxygen tank are presented that can be used as a guide for conducting similar analyses on future launch vehicles. A typical prelaunch loading condition with combined thermal and mechanical loads is considered, and applications of the advanced modeling and analysis capabilities to linear bifurcation buckling and nonlinear static analyses are presented. The results for this problem illustrate a localized short-wavelength bending response, and that a high-fidelity model is required to represent accurately the behavior. A mesh refinement strategy is presented that is based on the linear bifurcation buckling analyses and does not require respecification of the shell wall properties and loads. Specifically, mesh refinement is simplified by using user-written subroutines to describe the spatial distribution of complex shell wall properties and loading conditions. In addition, a procedure for assessing the sensitivity to initial shell wall geometric imperfections is presented. For the prelaunch load condition considered, the deformations from a nonlinear analysis using these capabilities are found to be similar in shape to the linear bifurcation buckling mode shape and insensitive to initial geometric imperfections. Recommended solution procedures for large-scale nonlinear analysis include using an arc-length projection method, and a combination of modified and true Newton refactoring schemes to balance computational efficiency and robustness, with careful monitoring of the stability of the obtained solutions.

Introduction

THE International Space Station (ISS) is currently planned to occupy a 51.6-deg orbit. Construction of the ISS will require the Space Shuttle to deliver a large number of payloads to this high-inclination orbit. However, achieving this orbit requires that the payload capacity of the orbiter be reduced by approximately 10,000 lb. To recover part of this lost payload capacity, and to minimize the number of Space Shuttle flights needed to build the ISS, NASA developed a new, lighter-weight external fuel tank for the Space Shuttle. This new design, referred to as the superlightweight (SLWT) external tank, is made primarily of an aluminum–lithium alloy and weighs approximately 58,000 lb, which is approximately 8000 lb lighter than the lightweight aluminum external tank previously in service. This 8000 lb weight savings translates into an 8000 lb increase in the payload capacity for the orbiter. The new SLWT tank flew for the first time on 2 June 1998 (Space Transportation System-mission 91).

An important consideration in the design of the SLWT tank is the nonlinear behavior of its thin-walled regions that experience compressive or shear stresses, and the sensitivity of this behavior to initial geometric imperfections. Small initial geometric imperfections are known to sometimes cause premature buckling of thin shell structures. These effects are very important because local or global buckling of the SLWT tank shell wall could lead to catastrophic structural collapse or cause the thermal protection system (TPS) to separate from the tank, which could also cause the vehicle to fail. To eliminate shell-wall instabilities for operational loads, accurate predictions of the nonlinear response and imperfection sensitivity of the SLWT tank are needed.

One thin-walled component of the SLWT tank that experiences significant compressive stresses is the liquid-oxygen (LO_2) tank (see Fig. 1). Prior to launch, the weights of the liquid-hydrogen (LH_2) tank, the LO_2 tank, and the fuel induce reactions at the solid-rocket-booster attachment points that cause meridional compressive stresses and shear stresses that extend into the nose of the SLWT tank. The tank also experiences similar compressive and shear stresses during ascent, before the two solid rocket boosters (SRBs) are jettisoned. After the SRBs are jettisoned, and prior to orbital insertion, the LO_2 tank experiences compressive stresses in the aft end of the tank instead of in the nose region. Extensive modeling studies and nonlinear analyses of the LO_2 tank have been conducted at the NASA Langley Research Center. The nonlinear behavior of the SLWT LO_2 tank subjected to two critical prelaunch loading conditions and two critical flight loading conditions has been documented extensively in Refs. 1–4. In these references, accurate predictions of the nonlinear response of the SLWT tank have been shown to require a large-scale, high-fidelity, finite element model to represent complex structural details and a robust nonlinear shell analysis capability that can predict local and general instability buckling modes.

The objective of the present paper is to describe the modeling and analysis techniques that were employed by NASA to predict accurately the nonlinear response of the LO_2 tank subjected to combined mechanical and thermal loads. The structural configuration and the loading conditions are typical of a large-scale launch vehicle, and the modeling and analysis methods used should be of interest to analysts responsible for interrogating the nonlinear structural response and imperfection sensitivity of future launch vehicles. Because the present paper's intention is to describe the analysis of the SLWT LO_2 tank as a demonstration of generic techniques that can be applied to other structures, explicit details of the structure and load values have been omitted from this paper. Rather, an overview of the SLWT tank structure and loading conditions is presented, followed by a description of the modeling approach and specialized modeling

Received 22 April 1998; revision received 23 July 1999; accepted for publication 23 July 1999.

*Senior Structural Engineer, Structures and Acoustics Department; currently Aerospace Engineer, Mechanics and Durability Branch. NASA Langley Research Center, Hampton, VA 23681. Member AIAA.
†Research Scientist, Materials and Structures Technology Department. Member AIAA.

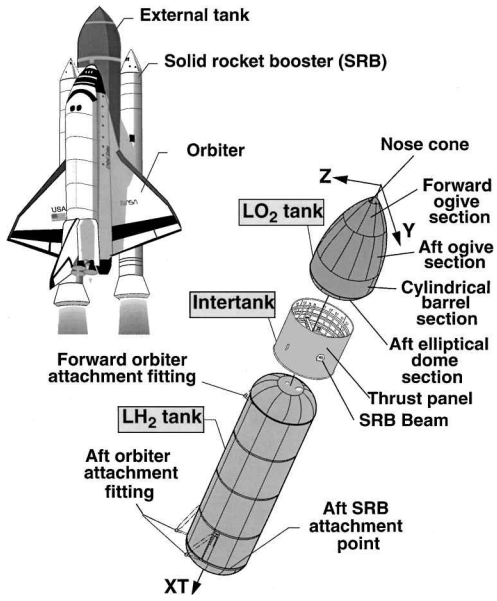

Fig. 1 Space Shuttle ET components.

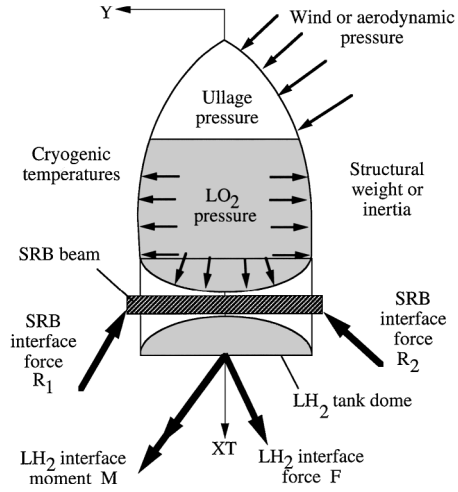

Fig. 2 General loading characteristics.

capabilities that were used to develop a large-scale, high-fidelity, finite element model that represented the structural features and complex loading. Analytical results are presented for a prelaunch loading condition to illustrate model development procedures and typical response characteristics. Results that illustrate the sensitivity of the nonlinear shell response to initial geometric imperfections are also presented. Specific recommendations for model development, analysis procedures, and solution control parameters, formulated based on the experience of the authors during the course of this work, are described that may be generally applicable to the analysis of future launch vehicles.

Overview of the Structure and Loading Conditions

The Space Shuttle consists of the Orbiter, two SRBs, and the external tank (ET) as shown in Fig. 1. The ET consists of an LO_2 tank, an LH_2 tank, and an intertank structure (Fig. 1). The SLWT LO_2 tank is a thin-walled monocoque shell that is primarily made of 2195 aluminum–lithium alloy. The LO_2 tank is approximately 49 ft long and has a maximum diameter of approximately 27.5 ft. Nominal wall thickness is on the order of 0.1 in. As shown in Fig. 1, the LO_2 tank consists of a nose cone, a forward-ogive section, an aft-ogive section, a cylindrical-barrel section, and an aft elliptical dome section. Each section of the LO_2 tank is constructed of several gore or barrel panels that are stretch formed, chemically milled, and then welded together. The panels are fabricated with substantial thickness tailoring to reduce structural weight. The panels are made somewhat thicker at the welds to form a stiffenerlike region that is used as a weld land. The weld lands are tapered in thickness and width along their length.

The intertank (see Fig. 1) is a right circular cylinder that is made from 2090 and 7075 aluminum alloys. It is approximately 22.5 ft long and has a diameter of approximately 27.5 ft. The intertank consists of eight stringer-stiffened panels that are fastened to five large internal rings. A large tapered beam, referred to herein as the SRB beam, spans the diameter of the intertank at the central ring and connects the intertank to the solid rocket boosters. The stringer-stiffened panels of the intertank that are attached to the SRB beam are called thrust panels. Loads on the SRB beam are diffused into the intertank and then into the LO_2 tank shell wall through these thrust panels.

Several critical SLWT tank loading conditions have been identified by the members of the SLWT tank team at the NASA Marshall Space Flight Center and the Lockheed Martin Michoud Space Systems Division. The general characteristics of the critical loads are shown in Fig. 2. The loads consist of wind pressure load, the structural weight, the pressure exerted on the shell wall by the LO_2, the ullage pressure inside the tank, the interface forces exerted by each SRB (indicated by $\boldsymbol{R}_1$ and $\boldsymbol{R}_2$ in Fig. 2), the interface forces between the intertank and the LH_2 tank (indicated by the vectors $\boldsymbol{F}$ and $\boldsymbol{M}$ in Fig. 2), and the loads associated with the cryogenic temperatures. The critical loading condition that is addressed in this paper corresponds to a prelaunch fueling condition that occurs when the Space Shuttle is still on the launch pad and the LH_2 tank and the LO_2 tank are both full of propellant. The SRB interface loads develop meridional compressive stresses in the LO_2 tank above the SRB attachment points that can cause the shell wall to buckle. In addition, circumferential or hoop tension stresses are generated by the hydrostatic LO_2 pressure that act to stabilize the shell wall. The meridional compression combined with hoop tension creates a short-wavelength instability in the aft-ogive section of the LO_2 tank.

STAGS Finite Element Analysis Code

The STAGS nonlinear finite element analysis code[5] was used in the present study to conduct nonlinear collapse analyses of the SLWT tank. The STAGS code was chosen for analyzing the SLWT tank because of its robust state-of-the-art, nonlinear-equation solution algorithms and its general user-input capability that is convenient for modeling branched shells typically used for launch vehicles.

Modeling

STAGS is a finite element analysis code specifically tailored for analyzing branched shell structures. Finite element models developed for STAGS are defined by use of the following:

1) Shell units are thin plate or shell geometric surfaces. They have local surface coordinate systems and are comparable to patches in graphical preprocessors. Discretization is defined by a numbering system based on rows of columns.

2) Element units are individually defined nodes and finite elements. If a graphical preprocessor is used, the model is translated into a STAGS element unit.

STAGS has been interfaced with PATRAN and IDEAS for graphical pre- and postprocessing. The models presented in the current paper were developed in shell unit/element unit format with heavy use of user-written subroutines. A graphical preprocessor was not used, but PATRAN was used for graphical postprocessing. STAGS also includes its own graphical postprocessor that produces plots in postscript and Acrobat™ formats.

STAGS permits use of user-written subroutines to model complex geometry and loading conditions in a direct manner that is essentially independent of mesh discretization. Descriptions and simple examples of the STAGS user-written subroutines are provided in Chapter 9 of the STAGS Users Manual.[5] The user-written subroutines are written in FORTRAN and allow structural parameters or loads to be computed at each integration point in the model, based on shell unit number, shell surface coordinates, or global Cartesian coordinates. In modeling the SLWT tank, the STAGS user-written subroutines LAME, WALL, CROSS, TEMP, and UPRESS were

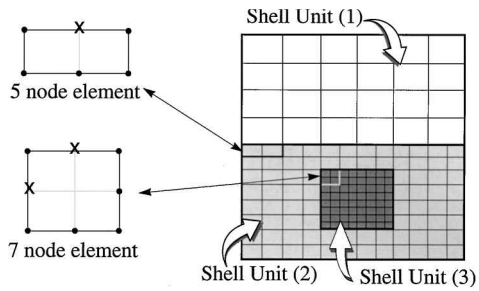

a) STAGS transition elements **b) Mesh refinement example**

Fig. 3 Transition elements and mesh refinement.

used to define the ogival meridian geometry, tapered shell walls and stiffener cross sections, and complex temperature and pressure distribution functions, respectively.

Imperfections

The nonlinear response of thin-walled shells can be very sensitive to initial geometric imperfections. In the STAGS code, initial geometric imperfections in the shell reference surface can be defined by any combination of the following forms: trigonometric representation in terms of shell unit surface coordinates, general parametric representation using the DIMP user-written subroutine, and linear combination of eigenvectors from linear bifurcation buckling analyses.

Elements

The STAGS element library includes two-noded beam elements, shell elements (triangular plate, four-noded von Kármán plate, five-noded and seven-noded von Kármán plate transition elements, and nine-noded first-order shear shell), and specialized elements (rigid links, mounts, hyperelastic fasteners, and contact). In STAGS version 3.0, a sandwich element and several solid elements were introduced. The finite element models used in the present study are constructed of beam elements, and von Kármán plate elements that are based on classical thin-shell theory. The plate element used is described in Ref. 6. The use of elements based on thin-shell theory is justified from a practical perspective because the ratio of the wall thickness to the minimum radius of curvature at each point of the undeformed LO_2 tank is much less than 0.1, and, as will be shown, because the ratio of the largest thickness of the shell wall that forms a given deformation pattern to the smallest characteristic length of the deformation pattern is less than 0.1 (see Refs. 7–9).

Mesh Refinement

The five-noded and seven-noded transition elements are shown in Fig. 3a. These elements are used to connect groups of four-noded plate elements with a 2–1 mesh refinement. There are two methods for locally increasing the mesh refinement in a STAGS model built from shell units. The first method is demonstrated by shell units 1 and 2 in Fig. 3b. These adjacent shell units are connected along shell unit edges that are coincident, and the edge of shell unit 2 is meshed twice as fine as the edge of shell unit 1. To make the connection, five-noded transition elements are introduced in shell unit 2. The second method to introduce mesh refinement is demonstrated by shell units 2 and 3 in Fig. 3b. First, a cutout is prescribed in shell unit 2 to eliminate a region of elements in the coarse mesh. Then, shell unit 3 is defined to fit into the cutout region and have twice the refinement of the coarse mesh it is replacing. The two shell units are connected by STAGS transition elements in shell unit 3; that is, five-noded elements on the straight edges and seven-noded elements in the corners.

Specialized Features

Two specialized features used in this study are moving plane boundaries and least-squares distributed line loads. A moving plane boundary is like an ordinary symmetry condition, except the plane of symmetry can translate and rotate. A group of nodes that lie on a moving plane boundary are constrained to deform such that they remain in a common plane.

A least-squares distributed line load is a boundary constraint function that is used to apply equivalent beam loads to the boundary of a thin-shell, finite element model without artificially distorting the shell wall. To specify a least-squares load, a group of nodes on the thin-shell surface and a reference node are identified. A section image of the undeformed cross section of the nodes on the thin-shell surface is defined and tied to the reference node. During the analysis, equivalent beam loads (point forces and moments) are applied to the reference node, and the reference node translates and rotates with the section image tied to it. A constraint function is then applied to minimize, in a least-squares sense, the displacements of the nodes on the thin-shell surface relative to the section image tied to the reference node. The least-squares function is weighted by the section stiffness of the thin-shell structure. By using this least-squares constraint function, the resultant loads applied at a single point are smoothly distributed into the thin-shell structure.

Analysis

STAGS is capable of conducting strength, stability, and collapse analyses for general shell structures, and can account for both geometric and material nonlinearity. To obtain the solution to complex nonlinear problems, STAGS uses both the modified and full Newton methods for its nonlinear solution algorithms and accounts for large rotations in a shell by using a corotational algorithm at the element level. STAGS has static and transient analysis capabilities that can be used to predict local instabilities and modal interactions that occur due to the addition of destabilizing mechanical loads such as an applied compression or shear load. The Riks pseudo-arc-length path following method[10,11] is used to continue a solution past the limit points of a nonlinear response. There are two solvers available in the STAGS code: the original Skyline solver and a recently added sparse matrix solver. The sparse matrix solver is significantly faster than the Skyline solver for problems with more than 20,000 degrees of freedom (DOF). The solution strategy used to obtain the results presented in the current study will be explained in detail.

Development of the Finite Element Model

A finite element model of the LO_2 tank and the intertank was created. The majority of the structure was modeled as an assembly of discretely stiffened monocoque shells. Because the focus of the present study was the response of the LO_2 tank, the heavily stiffened components in the intertank were represented by shells with equivalent smeared stiffener properties, defined by using the smeared stiffener modeling feature in STAGS.[5] The smeared stiffener approximation provided a good representation of the intertank stiffness and load transfer into the LO_2 tank, without introducing too much detail into the intertank model. When designing the model, it was recognized that the same basic model would be used for several load cases. Each load case would require different regions of the model to be finely meshed. To make it easy to tailor the mesh for each load case, the geometric model, structural properties, loads, and boundary conditions were defined independent of the mesh discretization.

Geometry

The geometry of the SLWT tank model was defined using STAGS shell units. The reference surface of each shell unit was selected to coincide with the nominal midsurface of the shell wall, as opposed to selecting the inner radius as the reference surface, for example. By locating the reference surface at the nominal midsurface of the shell wall, membrane-bending stiffness coupling caused by shell wall eccentricities is minimized, which simplifies the nonlinear response and provides for faster convergence of the solution as the finite element mesh is refined. All geometries, except the ogive geometry of the LO_2 tank, were described in the model setup input file using standard shell surfaces (cylinders, cones, annular plates, ellipsoids, and spheres). The ogive surface geometry was input directly into the STAGS code with the user-written subroutine LAME. This subroutine is used to prescribe the proper differential geometry of a nonstandard reference surface. The geometric model of the LO_2 tank and the intertank is shown in Fig. 4.

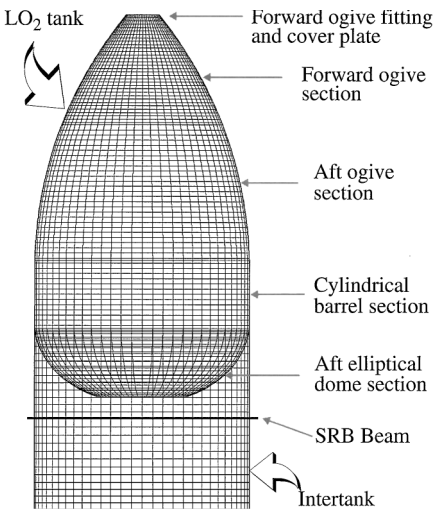

Fig. 4 Geometric model of the LO_2 tank and intertank; mesh shown has 49,000 DOF.

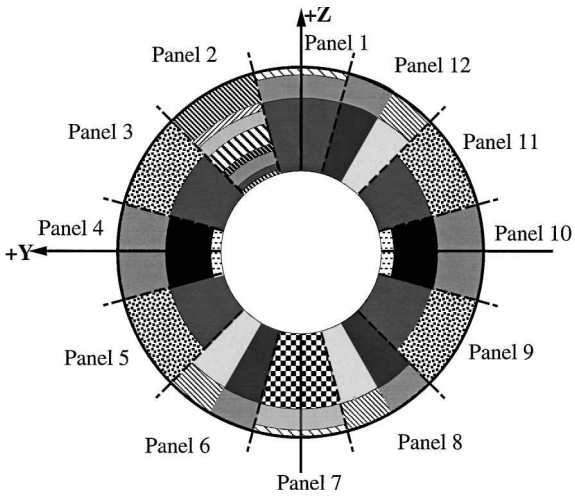

Fig. 5 Planform view of aft-ogive thickness map.

Beam Cross Sections and Shell Wall Fabrications

Nearly every panel of the SLWT tank has substantial thickness tailoring to reduce structural weight. This made the task of assigning structural properties quite involved. Standard beam cross-sectional properties and shell wall fabrication properties were described in the model setup input file, while beam and shell wall properties that varied spatially were specified in user-written subroutines CROSS and WALL, respectively. For example, these subroutines were used to assign properties in the aft-ogive section. The geometry of the aft ogive was modeled with a single shell unit, and the actual structure is constructed from twelve gore panels that are stretch formed, chemically milled, and welded together. The complexity of the thickness map is demonstrated by a sketch of the 12 aft-ogive gore panels shown in Fig. 5. In Fig. 5, regions with different thickness have different fill patterns. There are regions of uniform and linearly varying thickness, and there are thickness discontinuities. The spatial variation in shell wall thickness was coded in FORTRAN in the user-written subroutine WALL by using conditional statements to assign shell wall properties depending on the location in the structure. This WALL subroutine is called during the analysis to compute shell wall properties at each integration point of the finite elements. Note that, if a coarse mesh is prescribed, integration points are widely spaced, and local variations in thickness will not be detected. For this reason, subroutine WALL should not be used to model narrow strips of thickened material. In the current model, the thickened weld lands between the gore panels are modeled as discrete beams. The weld lands are tapered in thickness and width along their length, and the user-written subroutine CROSS was used to assign beam cross-sectional properties that reflect this taper.

Loads

The loads shown in Fig. 2 were prescribed through input in the standard model setup input file and with the additional user-written subroutines TEMP and UPRESS. The user-written subroutines were coded in FORTRAN to compute the spatial variation of loads, independent of the mesh. Cryogenic temperature distributions over the entire structure were prescribed in the user-written subroutine TEMP. The wind loading, ullage pressure, and LO_2 inertial loads on the LO_2 tank surface were represented by pressure loads prescribed in the user- written subroutine UPRESS. The wind load was computed from a Fourier series representation, the ullage pressure was constant, and the LO_2 pressure caused by $1g$ acceleration of the LO_2 was proportional to the distance from the LO_2 fill line. In the finite element model, all pressure loads are live loads that remain normal to the deformed element surface.

The remainder of the loads shown in Fig. 2 are applied in the standard model setup input file. The structural weight was included by applying a $1.0g$ inertial loading. The LH_2 interface loads represent resultant forces and moments on the intertank cross section. In STAGS, these resultants were applied by defining a least-squares loading constraint between all of the nodes at the end of the intertank, and a reference node in the center of the intertank cross section. The LH_2 interface forces and moments were then applied to the reference node. A moving plane boundary was also applied at the end of the intertank to minimize the effect of not modeling the LH_2 tank. Finally, the model was constrained against rigid-body motion by constraining all translations and rotations at both ends of the SRB beam. Thus, the SRB interface forces shown in Fig. 2 are manifested in the analysis as reactions to all the other loads. By constraining both ends of the SRB beam, elongation of the SRB beam is restrained, which does introduce some undesirable forces along the beam axis. The effects of these forces are negligible because they are contained within the central region of the intertank and the primary loading on the structure is perpendicular to the SRB beam axis.

Analysis Procedures for a Typical Load Case

Several critical SLWT tank loading conditions have been identified by the members of the SLWT tank team at the NASA Marshall Space Flight Center and the Lockheed Martin Michoud Space Systems Division. Because the analytical procedures were common for all load cases, only a single load case was considered in this paper. A general schematic for the prelaunch fueling condition when the LH_2 tank and the LO_2 tank are both full of propellant is shown in Fig. 2. The numerical results were obtained for the case where the wind load, the LO_2 pressure, the structural weight, and the temperature field were held constant, while the LH_2 interface loads are increased proportionally until buckling or wrinkling occurred. Representative results from linear bifurcation buckling analyses and nonlinear collapse analyses of the SWLT are shown in Figs. 6–11. In the present study, the stress levels were always below the approximately 70-ksi yield stress of the aluminum–lithium material, and so an elastic analysis only was considered. For a more detailed description of the structure, the loading, and the numerical results, see Ref. 1.

Load Sets

Loading in STAGS can be specified in two load sets, load set A and load set B. The load factors applied to each load set, *PA* and *PB*, respectively, can be varied independently. For collapse analyses, it is common to place passive loads (loads that will be held constant) in load set B, and to place the active loads (destabilizing loads that will be varied) in load set A.

In STAGS, if a linear bifurcation buckling analysis is executed from a linear prestress state with two load sets, load factor *PB* is held constant, and the eigenvalue is applied to load factor *PA*. Therefore, the critical load obtained will be

$$\text{load}_{\text{cr}} = \lambda_{\text{cr}} PA(\text{load set A}) + PB(\text{load set B}) \qquad (1)$$

To run a nonlinear collapse analysis, nonlinear solutions are obtained with load factors *PA* and *PB* increasing together. When *PB*

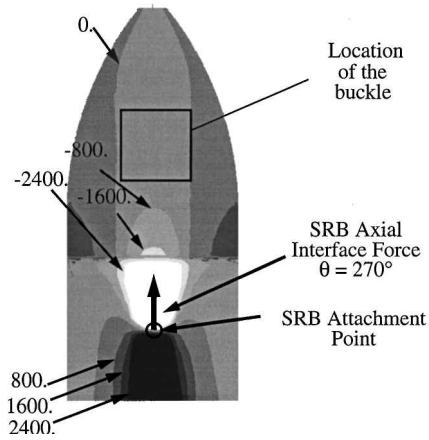

a) Meridional stress resultant (lb/in.)

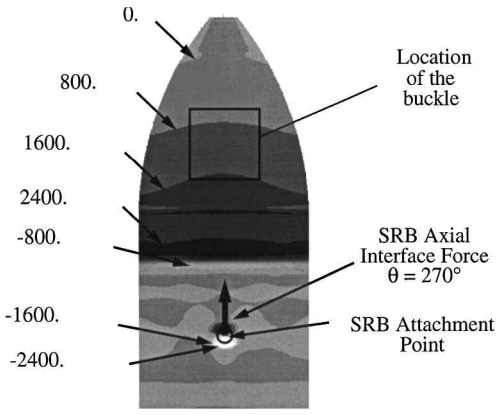

b) Circumferential stress resultant (lb/in.)

Fig. 6 Stress resultants from the linear prestress solution (*PA* = *PB* = 1.0) of the 49,000-DOF model.

reaches a load value associated with nominal loading, then *PB* is held constant while load factor *PA* continues to increase. The results are for analyses with the LH_2 interface loads on load set A and all other loads on load set B.

Linear Bifurcation Buckling Analyses and Mesh Refinement

The finite element model of the SLWT tank consists primarily of a geometrical model that is virtually independent of the mesh. To define a mesh that is sufficient to obtain an accurate nonlinear solution with the onset of a short-wavelength instability, the following procedure is followed:

1) Initially, a coarse mesh is prescribed and a linear bifurcation buckling analysis is conducted. The linear prestress solution is examined to verify that loads and boundary conditions are properly applied. Shell element stress resultants are plotted to display load paths, and the linear eigenvectors indicate buckling critical areas that may require mesh refinement. The rule of thumb in STAGS for mesh refinement is that the final mesh should have at least four elements per half wave of the buckle pattern.

2) The mesh is modified to increase the refinement of compression loaded regions that may be buckling critical. The refined region should be large enough to include any potentially critical modes. (Focusing too early on one location may cause the true critical location to be obscured by a coarse mesh.) Mesh transitions are introduced to reduce the refinement of noncritical regions and add refinement in critical regions.

3) A linear bifurcation buckling analysis is conducted with the new mesh, and the linear eigenvector is reviewed.

4) Steps 2 and 3 are repeated until the eigenvalue converges and the eigenvector is smoothly represented by the local mesh.

The implementation of this procedure is now demonstrated for the prelaunch loading condition. A coarse mesh was prescribed,

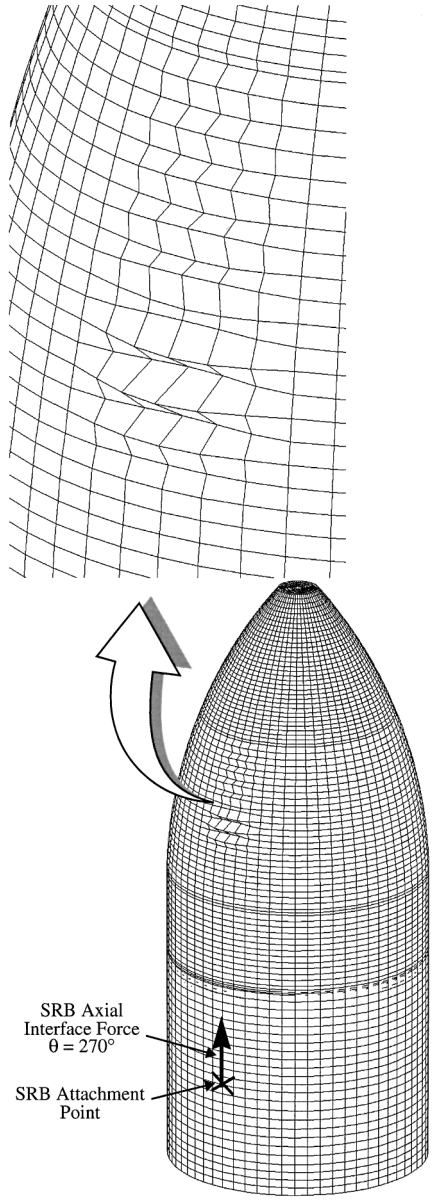

Fig. 7 Buckling mode for the 49,000-DOF model; PA_{cr} = 4.22 and *PB* = 1.0.

and a linear bifurcation buckling analysis associated with increasing the LH_2 interface loads was conducted. The coarse mesh had 49,000 DOF and is shown in Fig. 4. Contours of the meridional and circumferential stress resultants from the linear prestress solution with $PA = PB = 1.0$ are shown in Fig. 6.

The model is viewed from the negative Y-axis side ($\theta = 270$ deg) of the tank, and the stress resultants are given in pounds per inch. The results in Fig. 6a show that there are compressive meridional stresses in the model at $\theta = 270$ deg from the SRB attachment point up into the nose cone. The results in Fig. 6b show that there are tensile circumferential stress resultants in the LO_2 tank. When the LH_2 interface loads are increased, the compressive meridional stresses increase. The linear bifurcation buckling analysis of the 49,000-DOF model predicted that buckling would occur in the aft-ogive section at the location indicated in Figs. 6a and 6b. In this region of the LO_2 tank, the compressive meridional stress and tensile circumferential stress combine to create a short-wavelength buckling mode.

The mode shape predicted by STAGS for the 49,000-DOF model is shown in Fig. 7 and corresponds to a critical load factor for the LH_2 interface loads with $PA = 4.22$. This mode shape prompted mesh refinement in the forward-ogive and aft-ogive sections of the LO_2 tank in regions centered above each SRB beam attachment point. Mesh refinement was accomplished by prescribing cutouts, or areas in

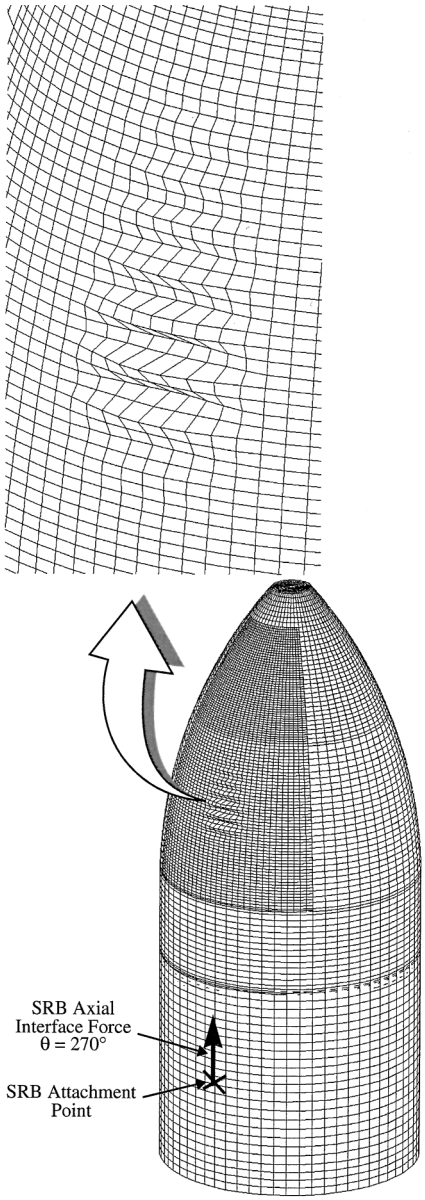

Fig. 8 Buckling mode for the 80,000-DOF model; PA_{cr} = 3.94 and PB = 1.0.

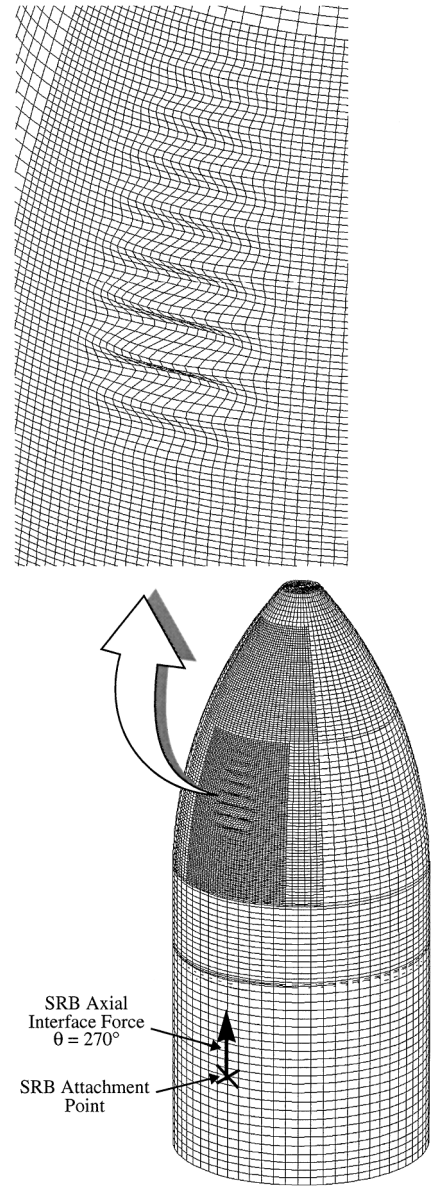

Fig. 9 Buckling mode for the 99,000-DOF model; PA_{cr} = 3.78 and PB = 1.0.

the coarse mesh that were eliminated. Then additional shell units were defined which fit into the cut-out regions and had twice the refinement of the coarse meshes they were replacing. STAGS transition elements were then used to mate the inserted fine meshes to the surrounding coarse mesh. The new mesh, with one level of mesh refinement, had 80,000 DOF. The mode shape predicted by STAGS for this model is shown in Fig. 8 and corresponds to a critical load factor for the LH_2 interface loads with $PA = 3.94$. Another level of mesh refinement was introduced in the aft-ogive section to provide the final model with two levels of mesh refinement and 99,000 DOF. The linear bifurcation buckling mode for this model is a short-wavelength wrinkle in the aft ogive, as shown in Fig. 9 and corresponds to a critical load factor of $PA = 3.78$. The smoothness of the buckling mode, and the 4% reduction in the eigenvalue from the previous mesh, indicates that this mesh is sufficient to represent the short-wavelength instability associated with this structure and loading condition. In addition, the ratio of the largest thickness in the area of the buckling mode shown in Fig. 9 to its smallest characteristic length is less than 0.1, which suggests that finite elements that are based on classical thin-shell theory are adequate.

The objective of the mesh refinement procedure was to develop a mesh that would adequately model the behavior with as few DOF as possible, to reduce the computational time and disk space requirements. While developing these models, it was noted that using transition elements increases the bandwidth of the problem, and thus can increase the computational time.

Nonlinear Analyses: Typical Results

Nonlinear analyses for the prelaunch loading condition were conducted using the 99,000-DOF model. Nonlinear solutions were obtained by increasing all loads simultaneously to a value of one ($PA = PB = 1.0$), then increasing the LH_2 interface loads while all other loads were held constant (PA increasing, $PB = 1.0$). Analyses were conducted for the geometrically perfect shell and a geometrically imperfect shell with an imperfection-amplitude-to-wall-thickness ratio $A/t = 0.3$. The thickness t in the ratio A/t is the minimum-gauge wall thickness of the aft ogive and has a value equal to 0.100 in. The linear bifurcation buckling mode shown in Fig. 9 was used as the imperfection shape, and a negative amplitude was specified to obtain the strongest interaction between the membrane compressive stress and shell wall deformations. Representative results from the nonlinear analyses are shown in Figs. 10 and 11.

The normal displacement w of the aft-ogive surface along a meridional line above the SRB attachment point is shown by the solid lines in Fig. 10 for LH_2 interface loads less than and greater than the load values reported for linear bifurcation. The results shown in Fig. 10a are for the geometrically perfect shell, and the results in Fig. 10b

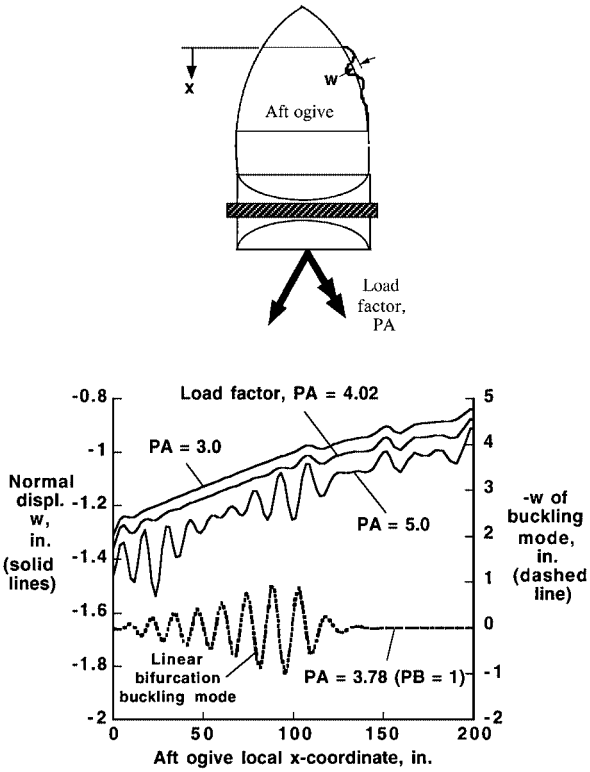

a) Geometrically perfect shell

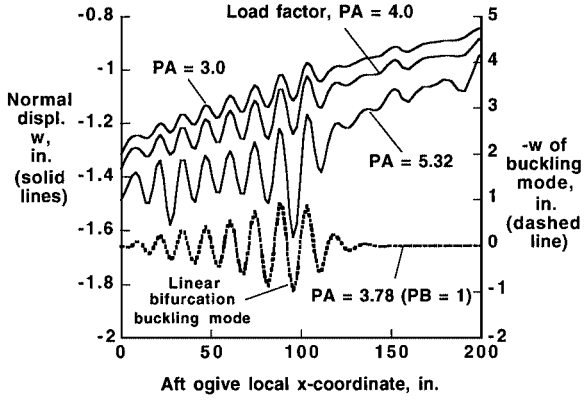

b) Geometrically imperfect shell: eigenmode imperfection with imperfection-amplitude to wall-thickness ratio $A/t = 0.3$

Fig. 10 Normal displacement w of the aft-ogive surface for increasing LH_2 interface loads, $\theta = 270$ deg.

are for the shell with the initial geometric imperfection. The linear buckling mode is shown in each figure by the dashed line. These results indicate that local bending gradients develop in the aft-ogive section as the LH_2 interface loads increase. The nonlinear analyses predict a short-wavelength response in the aft ogive that is very similar in shape to the corresponding linear bifurcation buckling mode shape. The short-wave response reiterates the need for a high-fidelity model to represent accurately the local bending behavior and hence predict short-wave bending gradients that may cause the TPS to separate from the shell wall in this region. The deformation patterns shown in Fig. 10 confirm that the ratio of the largest thickness in the area of the deformation to the smallest characteristic length of the deformation pattern is less than 0.1, which suggests that finite elements that are based on classical thin-shell theory are adequate. In addition, the von Mises stresses in the forward ogive and the barrel were calculated for the higher load factors shown in Fig. 10 and were found to be below the approximately 70-ksi yield stress of the aluminum–lithium material.

If the local displacement amplitude Δw is defined as the maximum difference in w for adjacent locations on the aft-ogive surface,

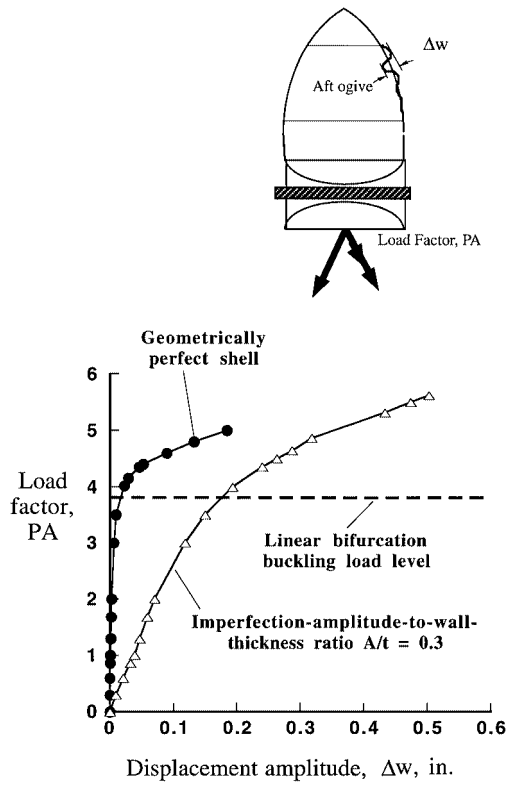

Fig. 11 Local displacement amplitude Δw of the aft-ogive surface for increasing LH_2 interface loads, $\theta = 270$ deg; geometrically perfect and geometrically imperfect shells.

then the growth of Δw with increasing LH_2 interface loads is shown in Fig. 11. The results shown in Figs. 10 and 11 indicate that the amplitude of local bending gradient increases rapidly for values of load greater than the linear bifurcation buckling load, and that shells with initial geometric imperfections can display substantial bending gradients even at relatively low loads.

Solution Control for Nonlinear Analyses

Running large nonlinear analyses can become expensive and time consuming, and so special care must be taken in setting solution control parameters. As demonstrated in Fig. 11, the geometrically perfect shell experiences a dramatic change in the solution behavior when the structure buckles. This change in behavior makes tracing the nonlinear response more difficult. As an aid to other analysts in conducting similar studies, the following general recommendations for solution control were formulated based on the experience of the authors during the course of this work.

The Riks pseudo-arc-length path following method[10,11] should be used for all solutions. This procedure is often advocated for continuing a solution past a limit point, but it is very effective anytime that the displacement field changes rapidly for small changes in load. This type of behavior was displayed in Fig. 11 for load values greater than the linear bifurcation buckling load.

During a nonlinear analysis, the STAGS code automatically adjusts the load (arc-length) increment for the next solution based on the convergence behavior of previous solutions. The linear nature of the response for loads less than the buckling load can cause STAGS to begin taking large increments in load prior to buckling. This may cause the solution to skip the first buckling mode and get on the wrong solution path. The STAGS code does allow the user to override the automatic incrementation and force a solution to be obtained at specified load factors. To prevent bypassing the nonlinear buckling response, load factors should be specified that are just below and just above the buckling load from a linear bifurcation buckling analysis. Also, if solution difficulties are encountered, the code will automatically cut the load increment and attempt to continue the solution, and the analyst controls the number of attempts by limiting the number of cuts in the loading, number of refactorizations,

or total run-time for the analysis. If the analyst observes that the solution is having difficulty, or solution difficulty is expected based on prior runs, then the analyst can terminate the run, and restart the analysis with a smaller load increment and more robust refactoring method. When conducting a nonlinear analysis, the majority of the computational effort is spent on forming and factoring the stiffness matrix. A true Newton method refactors on every iteration of every load step. This procedure is robust, but is very costly for large problems. A modified Newton method is recommended because it will refactor the stiffness matrix only when convergence difficulties are encountered. For maximum computational efficiency, a true Newton method should be used only when the modified Newton method fails. Conversely, if computer resources are abundant, and the analyst wants the highest likelihood of obtaining a nonlinear solution without having to monitor the progress of the solution (which is particularly useful when running analyses overnight or over the weekend), then an analyst may prefer to use the true Newton method for all analyses.

A warning should be issued regarding solutions obtained using the modified Newton method. Whereas the accuracy of a nonlinear solution (i.e. how well the solution satisfies the equilibrium equations) is the same whether a modified or true Newton method is used, the stability of the solution may be different. When examining the results of an analysis, the stability of a solution is judged by monitoring the number of negative roots obtained when factoring the stiffness matrix. Because the modified Newton method only refactors occasionally, not much information is supplied concerning the stability of solutions. The results of a single refactorization in the middle of a nonlinear analysis may indicate the stability of previous solutions, but the solutions obtained after the refactorization may be suspect. In conducting the analyses for this study, when a modified Newton method was used, the solutions that were obtained after the last refactorization were discarded because the stability of the solution may have been suspect. To minimize the risks of using the modified Newton method, there is a STAGS option that restricts the number of solutions obtained before refactoring.

Conclusion

The paper presents structural modeling techniques and results of nonlinear analyses of the Space Shuttle SLWT tank subjected to a typical prelaunch loading condition. Combined thermal and mechanical loads are considered, and the effects of initial geometric imperfections are included in the analysis.

The results have been used to illustrate the structural modeling and computational procedures needed, in general, to solve a large-scale, complex, nonlinear structural analysis problem of practical importance. An overview of the STAGS finite element analysis code was presented. The procedures that were used to develop a detailed finite element that could adequately simulate a local instability response were described. In addition, recommendations were made regarding solution control for large-scale nonlinear analysis. These recommendations include using an acr-length projection method, and a combination of modified and true Newton refactoring schemes to balance computational efficiency and robustness, with careful monitoring of the stability of the obtained solutions.

Acknowledgments

The authors would like to express their thanks to Michael P. Nemeth, Timothy J. Collins, James H. Starnes Jr., and Walter L. Heard Jr. (retired) of NASA Langley Research Center and Vicki O. Britt of Gulfstream Aerospace, Inc., for their technical support.

References

[1]Nemeth, M. P., Britt, V. O., Collins, T. J., and Starnes, J. H., Jr., "Nonlinear Analysis of the Space Shuttle Superlightweight External Fuel Tank," NASA TP 3616, Dec. 1996.

[2]Nemeth, M. P., Britt, V. O., Young, R. D., Collins, T. J., and Starnes, J. H., Jr., "Nonlinear Behavior of Space Shuttle Superlightweight Liquid-Oxygen Tank Under Prelaunch Loads," *Journal of Spacecraft and Rockets*, Vol. 36, No. 6, 1999, pp. 788–803.

[3]Young, R. D., Nemeth, M. P., Collins, T. J., and Starnes, J. H., Jr., "Nonlinear Behavior of Space Shuttle Superlightweight Tank Under Booster Ascent Loads," *Journal of Spacecraft and Rockets*, Vol. 36, No. 6, 1999, pp. 820–827.

[4]Nemeth, M. P., Young, R. D., Collins, T. J., and Starnes, J. H., Jr., "Nonlinear Behavior of Space Shuttle Superlightweight Tank Under End-of-Flight Loads," *Journal of Spacecraft and Rockets*, Vol. 36, No. 6, 1999, pp. 828–835.

[5]Rankin, C. C., Brogan, F. A., Loden, W. A., and Cabiness, H. D., "STAGS User Manual, Version 3.0," Lockheed Martin Missiles and Space Co., Rept. LMSC PO32594, March 1999.

[6]Rankin, C. C., and Brogan, F. A., "The Computational Structural Mechanics Testbed Structural Element Processor ES5: STAGS Shell Element," NASA CR 4358, May 1991.

[7]Simmonds, J. G., "An Improved Estimate for the Error in the Classical, Linear Theory of Plate Bending," *Quarterly of Applied Mathematics*, Vol. 29, No. 3, 1971, pp. 439–447.

[8]Stein, M., and Bains, N. J. C., "Postbuckling Behavior of Longitudinally Compressed Orthotropic Plates with Three-Dimensional Flexibility," AIAA Paper 86-0976, May 1986.

[9]Stein, M., "Effects of Transverse Shearing Flexibility on Postbuckling of Plates in Shear," *AIAA Journal*, Vol. 27, No. 5, 1989, pp. 652–655.

[10]Riks, E., "Some Computational Aspects of the Stability Analysis of Nonlinear Structures," *Computational Methods in Applied Mechanics and Engineering*, Vol. 47, Dec. 1984, pp. 219–259.

[11]Riks, E., "Progress in Collapse Analysis," *Journal of Pressure Vessel Technology*, Vol. 109, Feb. 1987, pp. 27–41.

H. L. McManus
Associate Editor